TiS Trends in Sciences
TRENDS IN SCIENCES 2027; 24(1): 14436
SPRINT Scholarly Publishing and Repository Integration Center
https://doi.org/10.48048/tis.2027.14436
RESEARCH ARTICLE

# Synthesis of Ternary Chitosan–$Al_2O_3$–Graphene Oxide Composite via Sol-Gel Method for Enhanced Adsorptive Removal of Methylene Blue: Characterization, Kinetics, and Isotherm Studies

**Desnelli[1,2,*], Fenti Apriyani[1], Daniel Alfarado[1,3], Eva Musifa[1], Muhammad Said[1,2], Ady Mara[1], Suheryanto[1], Wiwien Andriyanti[4] and Bayu Mardi Kartika[4]**

*[1]Department of Chemistry, Faculty of Mathematics and Natural Science, Universitas Sriwijaya, Sumatera Selatan, Indonesia*
*[2]Research Centre of Advanced Material and Nanocomposite, Faculty of Mathematics and Natural Science, Universitas Sriwijaya, Sumatera Selatan, Indonesia*
*[3]Chemistry Education Laboratory, Faculty of Teaching and Education, Sriwijaya University, Sumatera Selatan, Indonesia*
*[4]Research Centre for Food Technology and Processing, National Research and Innovation Agency, Yogyakarta, Indonesia*

**([*]Corresponding author's e-mail: desnelli@unsri.ac.id)**

*Received: 19 May 2026, Revised: 22 June 2026, Accepted: 15 July 2026, Published: 30 August 2026*

**Abstract**

The rapid growth of the textile industry has worsened water pollution with the release of synthetic dyes, especially methylene blue, which presents significant environmental and health risks due to its persistence against natural degradation. Graphene oxide (GO) has been proposed as a promising adsorbent. However, its practical application is constrained by post-treatment separation and secondary pollution, which can impede the overall effectiveness of employing GO in water treatment processes. The aim of this research was to synthesize a ternary composite of chitosan–$Al_2O_3$–graphene oxide (CS–AO–GO) via the sol-gel method for enhanced adsorptive removal of methylene blue and improved separation. The composite was prepared by adding GO and $Al_2O_3$ into the chitosan matrix with various mass ratios, and the ratio 1:3 (CS–AO–GO 1:3) was selected for detailed investigation due to its smaller crystal size. XRD characterization confirmed the successful incorporation of all 3 components. SEM-EDX revealed a porous heterogeneous surface morphology with elemental verification of carbon, nitrogen, oxygen and aluminum. BET analysis showed a significant enhancement in the specific surface area from 7.036 $m^2/g$ for pure chitosan to 23.009 $m^2/g$ for the composite, which had a mesoporous structure with an average pore size of 13.106 nm. Based on the batch adsorption study, the optimum conditions for methylene blue were obtained at pH 9, contact time 50 min and initial concentration 45 mg/L with an adsorption capacity of 10.817 mg/g and removal efficiency of 80.12%. The Langmuir isotherm model provided a good fit to the adsorption equilibrium data ($R^2 = 0.998$), indicating monolayer adsorption on a homogeneous surface with a maximum adsorption capacity of 11.600 mg/g. Kinetic studies showed that the adsorption process was found to follow a pseudo-second-order model ($R^2 = 0.982$), indicating that the rate-limiting step was controlled by chemisorption mechanisms such as electrostatic interaction, complex formation and π-π interaction. Results showed that the incorporation of $Al_2O_3$ and GO into the chitosan matrix significantly improved the surface area and adsorption efficiency, reaching almost six times as compared to pure chitosan. The synthesized CS–AO–GO composite is a promising and cost-effective and easily separable biopolymer-based adsorbent for the remediation of cationic dye-contaminated textile wastewater.

**Keywords:** Chitosan, Aluminium oxide ($Al_2O_3$), Graphene oxide, Sol-gel, Ternary composite, Methylene blue adsorption, Kinetics model adsorption, Isotherm model adsorption

**Introduction**

The swift expansion of the textile industry markedly exacerbates water pollution through the release of liquid waste containing toxic organic and inorganic substances [1]. Synthetic dyes are a significant pollutant due to their complex and stable aromatic molecular structures, which render them resistant to natural degradation and challenging to eliminate through conventional treatment methods [2]. Methylene blue, a prevalent cationic dye utilized in textile dyeing, is frequently discharged into the environment at elevated concentrations. The accumulation of methylene blue in aquatic environments not only compromises aesthetics and obstructs sunlight penetration for ecosystems but also presents significant health hazards to humans, including irritation, nausea, and methemoglobinemia upon ingestion [3]. Consequently, the formulation of effective and efficient remediation techniques for the extraction of methylene blue from wastewater has become an imperative requirement.

Graphene oxide (GO) has garnered significant interest recently as a novel adsorbent material for wastewater treatment technology, owing to its exceptional capacity to adsorb diverse pollutants [4]. The benefit of GO is attributed to its extensive specific surface area and the prevalence of polar oxygen functional groups (including hydroxyl, epoxy, and carboxyl) that facilitate its dispersion in aqueous environments [5,6]. However, the strong hydrophilicity and dispersibility of GO are major problems for batch adsorption applications. The small size of GO sheets and their high stability in colloidal suspension make it hard to separate and recycle the adsorbent after it has been used which could lead to secondary pollution from nanomaterial residues in treated water [7,8]. To address the challenges of separation while preserving the adsorption performance of graphene oxide (GO), researchers have increasingly utilized cross-linking strategies with biopolymers [9].

Chitosan was widely available renewable biopolymer obtained from the deacetylation of chitin found in crustacean waste, emerges as an excellent supporting matrix. The amino ($-NH_2$) and hydroxyl ($-OH$) groups present on the chitosan chain not only act as additional active sites for capturing dye molecules but also promote the formation of 3-dimensional composite structures that facilitate physical separation [10]. Rajabi and Jafari [11] in their study on GO-Chitosan/Glutaraldehyde (GO–CH/GLU) material for crocin dye application showed a separation efficiency of 94.17% in a continuous system, demonstrating the potential application of both industrial materials. Vo [12] revealed that chitosan–GO-based adsorbents can effectively absorb various organic dyes, including methylene blue, rhodamine B, Congo Red, and methyl orange, achieving absorption levels greater than 85%. Nevertheless, research by Desnnelli *et al.* [13] highlights that the chitosan–GO binary composite has limitations, specifically a relatively low specific surface area of only 11.60 $m^2/g$, which may limit both the rate and maximum adsorption capacity.

The efficiency of adsorption processes is fundamentally influenced by the available surface area of the adsorbent [14]. Consequently, modifications to the composite matrix are essential to enhance both porosity and active surface area. Metal oxides, especially alumina ($Al_2O_3$), are recognized for their excellent thermal and chemical stability, as well as their large specific surface area when synthesized at the nanoscale. It is hypothesized based on other studies that incorporating $Al_2O_3$ into the chitosan-GO matrix will not only significantly increase the composite's surface area but also improve its mechanical and thermal stability [15,16]. However, research on the synthesis and application of chitosan–$Al_2O_3$–GO ternary composites, produced via the sol-gel method for methylene blue removal, remains scarce and has not been thoroughly documented in the literature. This research aims to synthesize chitosan–$Al_2O_3$–GO composites using the sol-gel method, which was selected for its capability to produce materials with high homogeneity and purity at relatively low processing temperatures when the adsorption performance of the composite material was evaluated against methylene blue dye by varying key parameters. The findings of this study are anticipated to significantly contribute to the development of more efficient and easily separable biopolymer-based hybrid adsorbents for textile waste remediation applications

## Materials and methods

### Materials and instruments

The chemicals used in this research include graphite powder (size < 20 μm, purity ≥ 99%, Merck), chitosan (Merck), sodium hydroxide (pellets, ≥ 98%, Merck), hydrogen peroxide (30 %, Merck), potassium permanganate (≥ 99%, Merck), sodium nitrate (≥ 99%, Merck), aluminum nitrate nonahydrate (≥ 98%, Merck), oxalic acid dihydrate (≥ 99%, Merck), glacial acetic acid (Merck), sulfuric acid (96%, Merck), ammonia solution (25%, Merck), absolute ethanol (Merck), and methylene blue dye (Merck). The equipment utilized in this research comprises a UV-Vis spectrophotometer (Orion Aquamate 8000). Material characterization was conducted using an X-ray diffractometer (XRD, PANalytical X'Pert PRO) with Cu-Kα radiation (λ = 1.5406 Å) across a 2θ range of 5° - 80°, SEM-EDX (Thermo Fisher Scientific Phenom P-Series), and a surface area analyzer employing the Brunauer-Emmett-Teller (BET) method with nitrogen adsorption at 77 K across 20 iso points.

### Experimental procedure

#### *Synthesized materials of graphene oxide*

The synthesis of graphen oxide (GO) was carried on based on Anuwongsa *et al.* [17] with modification on preparation time. One g of graphite powder was oxidized with 50 mL of sulfuric acid at 80 °C and stirred for 24 h. Afterward, 1 g of $NaNO_3$ was added and agitated in a water bath for 1 h. The mixture was then placed in an ice bath (0 - 5 °C), and 6 g of $KMnO_4$ were gradually introduced portion-wise over the course of 1 h, maintaining the temperature below 10 °C. This was followed by the incremental addition of 3 g of $KMnO_4$ while stirring for an additional hour. A 30 mL solution of $H_2O_2$ was then added and diluted in a 250 mL volumetric flask. The solution was homogenized with a stirrer for 1 h. The resulting GO suspension was thoroughly rinsed by repeated centrifugation/washing until the pH approached neutrality. The washed GO cake was combined with demineralized water and dispersed through ultrasonic vibration for 1 h to separate the layers of GO. The exfoliated GO dispersion was subsequently heated at 80 °C in an oven for 4 h, resulting in solid GO.

#### *Preparation material $Al_2O_3$*

The synthesis of $Al_2O_3$ was conducted according to Buwono *et al.* [18] with some modification on process synthesis materials. Seven g of nonahydrate aluminum nitrate ($Al(NO_3)_3 \cdot 9H_2O$) were dissolved in 100 mL of 0.5 M hydrochloric acid. Next, 0.5 M ammonium hydroxide was added dropwise under continuous magnetic stirring (300 rpm) until the solution reached a pH of 9, forming a white gelatinous precipitate. The mixture was stirred for 4 h at 70 °C to complete gelation. The gel was then cooled, filtered, and the residue was rinsed with 96% ethanol and demineralized water. The washed gel was subsequently dried in an oven at 75 °C for 24 h. The resulting solid was ground into a fine powder and calcined in a muffle furnace for 6 h at 600 °C with a heating rate of 5 °C/min, yielding γ-$Al_2O_3$.

#### *Synthesis composite Chitosan−$Al_2O_3$−GO*

In a typical preparation, 0.5 g of solid GO was dispersed in 100 mL of aquademin and subjected to sonication in an ultrasonic bath (40 kHz, 100 W) for 15 min to achieve a uniform dispersion. Separately, 2.0 g of chitosan was dissolved in 100 mL of 1% (v/v) glacial acetic acid under stirring for 1 h, and 1.0 g of the calcined $Al_2O_3$ powder was suspended in 100 mL of demineralized water by stirring for 30 min. The chitosan solution and $Al_2O_3$ suspension were then added dropwise simultaneously to the GO dispersion under vigorous mechanical stirring (400 rpm). The mixture was stirred for 1 h at room temperature, after which the pH was adjusted to approximately 7 - 8 using dilute NaOH solution to precipitate the composite. The solid was collected by filtration, washed multiple times with deionized water until a neutral pH was reached, and dried at 80 °C for 4 h. The final composite (mass ratio chitosan:$Al_2O_3$:GO = 2:1:0.5) was ground and stored in a desiccator. To ensure batch-to-batch reproducibility, the entire synthesis was performed in triplicate; the 3 batches exhibited consistent XRD patterns with a coefficient of variation in crystallite size of less than 3%, and the methylene blue adsorption capacity (tested at 25 mg/L, pH 9, 60 min) varied by less than 5%.

### Methylene blue adsorption studies [20,21]

#### *Concentration determination for dyes*

The concentration of methylene blue in the solution is determined using UV-Vis spectrophotometry

at the maximum wavelength of 663 nm. A calibration curve, which illustrates the linear relationship between absorbance and methylene blue concentration within the range of 5 - 25 mg/L, serves as a reference for quantification. A stock solution of methylene blue at a concentration of 1,000 mg/L was prepared for all adsorption experiments.

***Point of zero charge (pHpzc)***

The point of zero charge (pHpzc) of the chitosan–$Al_2O_3$–GO composite was determined using the pH shift method. A total of 0.05 g of the adsorbent was dispersed in 50 mL of a 0.01 M NaCl solution, with the initial pH (pHi) adjusted to a range of 2 to 11 using 0.1 M HCl or 0.1 M NaOH. The suspension was agitated at 200 rpm for 2 h and then allowed to stand for 48 h to reach equilibrium. The final pH value (pHf) was recorded, and the pHpzc was determined from the intersection of the ΔpH (pHf - pHi) curve plotted against pHi.

***Evaluation of adsorption performance***

The adsorption efficacy of the chitosan–$Al_2O_3$–GO composite for methylene blue was evaluated in a batch system at ambient temperature. In each experiment, 0.05 g of adsorbent was added to 15 mL of methylene blue solution and agitated using an orbital shaker at a constant speed of 150 rpm. After the adsorption process, the suspension was allowed to rest for 60 min to enable the separation of the supernatant, which was then analysed for absorbance at a wavelength of 663 nm using a UV-Vis spectrophotometer. The equilibrium adsorption capacity (qe, mg/g) and the percentage removal (%R) were calculated based on the difference between the initial and final concentrations. The effect of solution pH was investigated by adjusting the initial pH of the methylene blue solution at 25 mg/L within the range of 7 to 11 (at one pH unit intervals) using 0.1 M HCl or 0.1 M NaOH prior to adding the adsorbent. The adsorption kinetics were assessed by varying the contact duration from 10 to 60 min at a fixed concentration of 25 mg/L. The adsorption isotherm was determined using initial methylene blue concentrations of 20, 25, 30, 35, 40, 45, and 50 mg/L, based on the optimal contact time established from the previous kinetic analysis. All experiments were conducted in duplicate to ensure data reproducibility. The adsorption absorption capacity is calculated using the Eq. (1):

$$\mathrm{Qe} = \frac{(\mathrm{Co} - \mathrm{Ce})}{\mathrm{W}} \times V \quad (1)$$

The initial concentration of methylene blue is represented by Co (mg/L), while Ce denotes the concentration of methylene blue that remains unadsorbed (mg/L). W signifies the weight of the composite used, and V indicates the volume of methylene blue employed. The percentage decrease in the concentration of methylene blue can be calculated using the Eq. (2).

$$\text{Efficiency adsorption } (\%) = \frac{(\mathrm{Co} - \mathrm{Ce})}{\mathrm{Co}} \times 100\% \quad (2)$$

**Data analysis**

**Characterization materials composite**

XRD analysis was conducted to determine the crystal size of the composite, resulting in a diffraction spectrum. The obtained spectrum was compared with the patterns recorded by the Joint Committee on Powder Diffraction Standards (JCPDS) and the International Centre for Diffraction Data (ICDD). The XRD diffraction pattern is presented as a function of 2θ, where θ represents the diffraction angle. The crystal dimensions of the chitosan–$Al_2O_3$–GO composite can be calculated using the Debye-Scherrer Eq. (3).

$$\mathrm{d} = \frac{\mathrm{K}\,\lambda}{\beta \cos\theta} \quad (3)$$

In the equation, d represents the crystal size in nanometres, k is a constant set at 0.9, λ denotes the wavelength of the X-ray used in the analysis, β indicates the full width at half maximum (FWHM) of the diffraction peak, and θ refers to the diffraction angle observed in the XRD diffractogram analysis spectrum. The chitosan–$Al_2O_3$–GO composite is examined using the BET apparatus to determine its surface area and pore dimensions. Following this, the chitosan–$Al_2O_3$–GO composite is characterised with the SEM-EDX instrument. The SEM analysis aims to investigate the surface morphology of the synthesised composite, while the EDX analysis provides information on the percentage composition of the test sample.

***Isotherm adsorption model***

The adsorption isotherm model used comprises the Langmuir and Freundlich isotherms, which are employed to determine the adsorption characteristics of the adsorbent. The following Eq. (4) illustrates the Langmuir isotherm for adsorption.

$$\frac{Ce}{Qe} = \frac{1}{Qm\ K_L} + \frac{1}{Qm} \quad (4)$$

where, qm is the maximum adsorption capacity (mg/g), KL is the Langmuir adsorption constant (L/mg). Thus, qm and KL are obtained from the intersection and slope of the linear plot between Ce/Qe and Ce. The Freundlich isotherm Eq. (5) is as follows:

$$\text{Log } Q = \log k + 1/n \log Ce \quad (5)$$

where, Ce is the equilibrium concentration of the adsorbate in the solution after adsorption (mg/L), k is the Freundlich adsorption constant, n is the empirical constant, and Q is the amount of adsorbate adsorbed per weight of adsorbent (mg/g).

***Kinetic adsorption studies***

Different kinetic models, including the pseudo-first-order, pseudo-second-order and intraparticle diffusion models, were applied to predict adsorption kinetics for the modified adsorbent. The best fit of the kinetics model is designated based on the linear correlation coefficient values. Lagergren's first-order kinetic equation is used to describe the solute adsorption on various adsorbents based on adsorbent capacity. This kinetcs model describes the adsorption rate and depends on the available sites in the adsorbent for physisorption process. The Lagergren first-order equation is expressed as Eq. (6):

$$\text{Ln } (Q_e - Q_t) = \text{Ln}Q_e - K_1 t \quad (6)$$

where, Qe and Qt are the amounts of methylene blue absorbed (mg/g) at equilibrium and at time (min), respectively; and K1 (min) is the first-order reaction rate constant. Pseudo-second-order by Ho describes the adsorption reaction rate with dependent energetically heterogeneous sites on the adsorbent; it is considered a chemisorption model. The pseudo-second-order equation is expressed as Eq. (7):

$$\frac{t}{Q_t} = \frac{1}{K_2 Q_e^2} + \frac{t}{Q_e} \quad (7)$$

where, $K_2$ (g/mg.min) is the rate constant of the second-order equation.

**Results and discussion**

**Charcterization material composite chitosan–$Al_2O_3$–graphene oxide (CS–AO–GO)**

***XRD characterization***

X-ray diffraction (XRD) analysis was conducted to determine the crystal structure and phases of each component of the composite, specifically chitosan, $Al_2O_3$, GO, and the chitosan–$Al_2O_3$–GO composite. **Figure 1** presents the diffractogram obtained from this characterization. The chitosan diffraction pattern (**Figure 1(a)**) shows distinct peaks at angles of 2θ = 20.86° and 40.36°, indicating the semi-crystalline structure typical of chitosan. The identified diffraction peaks are consistent with literature, which states that the primary peaks of chitosan fall within the 2θ range of 19° - 20°, correlating with the (110) crystal plane. This crystal plane originates from the organized arrangement of chitosan polymer chains, which are stabilized by both intramolecular and intermolecular hydrogen bonds. The broad nature of this peak reflects the coexistence of both ordered and disordered regions within the polymer matrix. Additionally, the secondary peak at approximately 2θ = 40° is generally associated with short-range order within the polymer matrix [22].

The diffractogram results for $Al_2O_3$, presented in **Figure 1(b)**, show distinct peaks at angles of 2θ = 37.96°, 45.82°, and 66.98°. These peaks correspond to the reflection planes (311), (400), and (440) of the γ-$Al_2O_3$ phase, which is characterized by a face-centered cubic structure. According to JCPDS standard data No. 29-0063, the characteristic peaks of γ-$Al_2O_3$ appear at angles of 2θ = 38°, 45°, and 67°. This indicates that the synthesis results in this study are closely aligned with the standard reference by Buwono *et al.* [18]. The presence of the γ-$Al_2O_3$ phase is advantageous due to its high specific surface area and the presence of active Lewis acid sites, which are beneficial for adsorption applications [23]. The sharp and well-defined peaks

confirm the high crystallinity of the synthesized alumina, which is essential for providing a stable and rigid framework within the composite.

The GO diffractogram (**Figure 1(c)**) shows a distinct peak at an angle of 2θ = 10.94°, which indicates the presence of graphene oxide resulting from graphite oxidation. This peak corresponds to the (001) plane of graphene oxide (GO) and confirms the successful exfoliation of graphite into GO sheets. The exfoliation is characterized by an increased interlayer distance due to the intercalation of oxygen functional groups. The peak at 2θ ≈ 10° - 11° has been widely documented in various studies as indicative of the transformation from graphite to graphene oxide (GO). The shift of the peak from 2θ ≈ 26° (for graphite) to a lower angle signifies an increase in interlayer distance from approximately 0.34 nm to about 0.8 nm, which is attributed to the incorporation of oxygen functional groups [22]. This expanded interlayer spacing is crucial as it facilitates the subsequent intercalation of chitosan chains and $Al_2O_3$ particles during composite formation. The difference in peak positions between chitosan (2θ = 20.86°) and graphene oxide (GO) (2θ = 10.94°) signifies inherent variations in their chemical structures and levels of crystallinity. Graphene oxide contains numerous oxygen functional groups, including carboxyl (−COOH), carbonyl (−C=O), epoxy (C−O−C), and hydroxyl (−OH). These groups increase interlayer spacing and lead to a shift in the diffraction peak to lower angles. In contrast, chitosan features carbon groups such as acetyl ($-COCH_3$) and amino groups ($-NH_2$), resulting in a semi-crystalline diffraction pattern marked by peaks at higher angles [24].

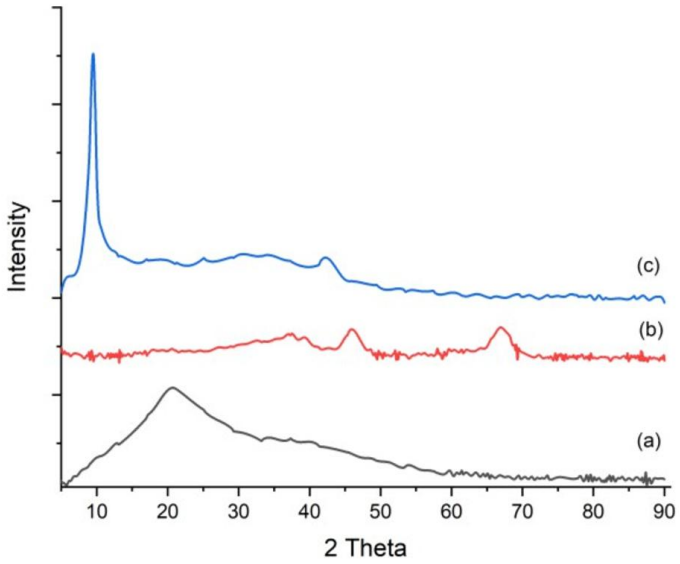



**Figure 1** XRD diffractogram of (a) chitosan, (b) $Al_2O_3$ and (c) GO.

The diffractogram of the chitosan–$Al_2O_3$–GO composite (**Figure 2**) shows a combination of peaks with reduced intensity, indicating the successful synthesis of the composite. Notably, the characteristic GO peak at 10.94° is completely absent in the composite diffractogram. This disappearance is strong evidence for the complete exfoliation and uniform dispersion of GO nanosheets within the chitosan–$Al_2O_3$ matrix, as the intercalation of polymer chains and nanoparticles disrupts the periodic stacking order of the GO layers. Sabzevari *et al.* [19] observed a similar phenomenon in the GO composite system cross-linked with chitosan (GO–CTS) and $Al^{3+}$ ions (GO–Al). The decrease in GO peak intensity within the composite suggests partial exfoliation of the GO sheets, which is attributed to the intercalation of chitosan chains and $Al_2O_3$ particles. This process enhances the accessibility of active sites for adsorption. XRD characterization was performed to investigate the effect of incorporating Graphene Oxide (GO) into the crystal structure of Chitosan- $Al_2O_3$ composites and Chitosan- $Al_2O_3$-GO composites, with mass ratios of (1:1), (1:2), and (1:3). The results of the

diffractograms are presented in **Figure 2**, and the calculated crystal sizes are summarized in Table 1. The diffractogram for the Chitosan- $Al_2O_3$ composite (**Figure 2(a)**) shows diffraction peaks at angles of 2θ = 25.59°, 35.14°, 37.74°, 43.34°, and 57.45°. These observed peaks correspond closely to the standard ICDD No. 01-075-1865 data (25.54°, 35.10°, 37.73°, 43.30° and 57.42°), confirming the successful integration of the $Al_2O_3$ crystalline phase within the chitosan matrix. Additionally, the interaction between chitosan and alumina particles within the composite matrix has been shown to modify the diffraction peaks indicating effective interfacial interactions [25].

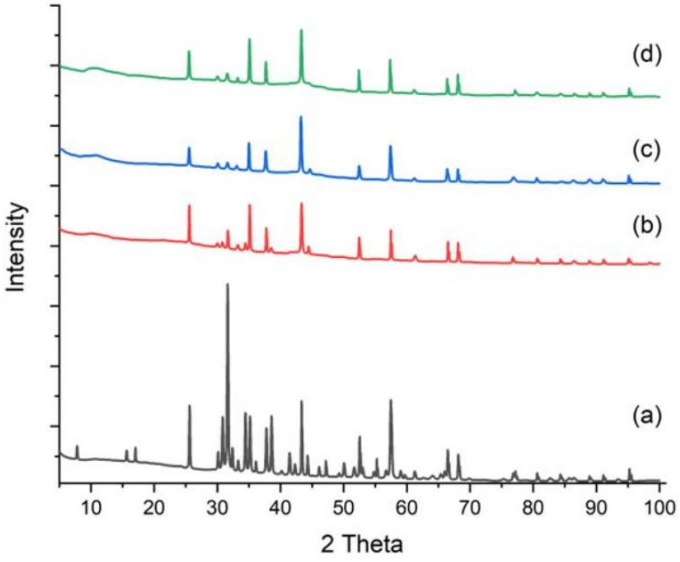



**Figure 2** XRD (a) chitosan–$Al_2O_3$, (b) chitosan–$Al_2O_3$–GO (1:1), (c) chitosan–$Al_2O_3$–GO (1:2) and (d) chitosan–$Al_2O_3$–GO (1:3).

**Table 1** Crystal size of graphene oxide and chitosan–$Al_2O_3$–GO composite with 3 ratios.

| Material | Crystal Size (nm) |
|---|---|
| Graphene Oxide (GO) | 2.360 |
| Chitosan–$Al_2O_3$–GO (1:1) | 9.431 |
| Chitosan–$Al_2O_3$–GO (1:2) | 5.210 |
| Chitosan–$Al_2O_3$–GO (1:3) | 5.082 |

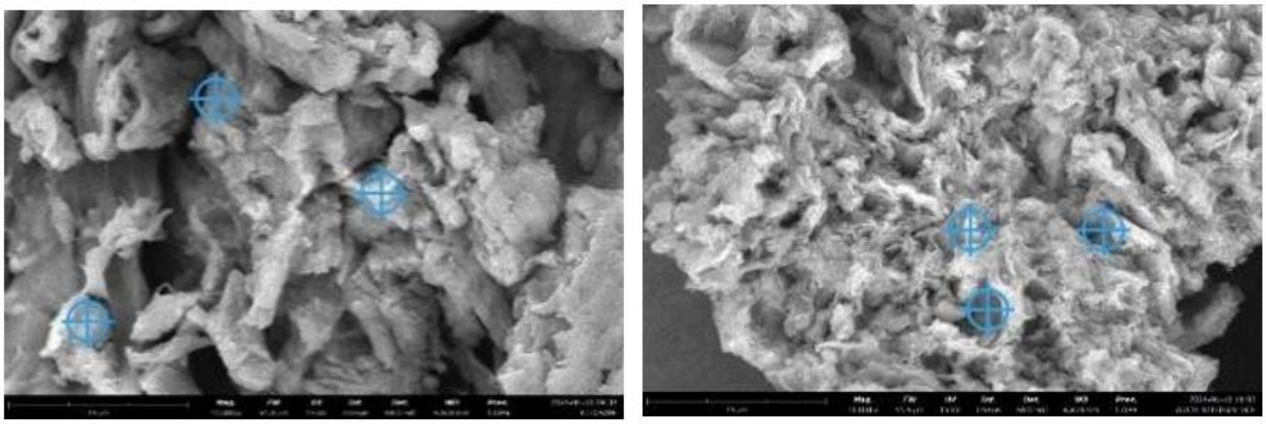
The incorporation of GO into the composite system results in significant changes to the diffraction pattern. In the chitosan–$Al_2O_3$–GO composite at a (1:1) ratio (**Figure 2(b)**), additional peaks were observed at 2θ = 31.65°, 52.45°, 66.50°, and 68.11°, alongside the peaks from $Al_2O_3$. The intensity of these new peaks became more pronounced with variations in the (1:2) and (1:3) ratios (**Figures 2(c)** and **2(d)**). The diffraction pattern of the composite with a (1:3) ratio closely resembles the standard ICDD No. 00-046-0943 data, particularly at the angles 2θ = 31.58°, 35.59°, 37.60°, 43.03°, 52.23°, and 66.22°. This suggests that a higher ratio of GO in the composite promotes the formation of new crystalline phases or, at the very least, enhances the overall order of the crystal structure. This indicates that GO acts not only as an exfoliated filler but also as a nucleating agent, promoting the reorganization of the polymer matrix and $Al_2O_3$ into a more ordered hybrid crystalline phase. A similar phenomenon has been observed by Saputra *et al.* [26], where the crystalline phase of GO is dominant within the biopolymer matrix indicating that the incorporation of GO significantly altered the crystallite size and induced micro-strain in the composite. The sharp diffraction peaks observed in the composite patterns are likely not exclusively derived from the chitosan–GO framework. These reflections can be attributed to crystalline $Al_2O_3$-related domains, although minor contribution from residual inorganic

species generated during the synthesis process cannot be completely excluded. This interpretation is consistent with the SEM-EDX results, which revealed trace amounts of Na, K, Mn, and S in the composite. Therefore, the XRD patterns are considered qualitative evidence of phase contribution and structural interaction among chitosan, $Al_2O_3$, and GO, rather than conclusive evidence of a highly crystalline polymer-based composite.

The subsequent examination of crystal dimensions (**Table 1**) reveals a clear relationship between the increase in GO mass fraction and the reduction in crystal size. The size of the composite crystals decreases progressively from the (1:1) ratio to the (1:3) ratio. This reduction in crystal size can be attributed to the role of GO as a heterogeneous nucleating agent. Graphene oxide sheets provide numerous nucleation sites, thus hindering the formation of large crystals and resulting in smaller more uniformly distributed crystallites within the composite matrix [27]. Mechanistically, the high surface area of GO provides an abundance of nucleation points, leading to a higher rate of crystal nucleation relative to crystal growth, which ultimately yields smaller crystallites. These findings are consistent with recent research showing that chitosan-GO composites produced via the hydrothermal method exhibit significantly smaller crystallite sizes (~6.2 nm) compared to pure chitosan, reinforcing the idea that GO enhances the crystalline properties of the composite. As a result, the chitosan–$Al_2O_3$–GO composite with a (1:3) ratio was chosen as the adsorbent for the subsequent methylene blue adsorption study. This choice is based on the fact that this composite has the smallest crystal size among the 3 variations. Chen *et al.* [28] suggest that smaller crystal sizes in an adsorbent are positively correlated with an increased adsorption rate, as smaller particle sizes offer a greater effective surface area for interaction with the adsorbate. The chitosan–$Al_2O_3$–GO (1:3) composite has the smallest crystal size of the 3 ratios, so in this study the chitosan–$Al_2O_3$–GO )1;3) composite was chosen for further characterization, namely SEM-EDX and BET, and was applied for the adsorption of methylene blue dye. Mechanistically, the high surface area of GO provides an abundance of nucleation points, leading to a higher rate of crystal nucleation relative to crystal growth, which ultimately yields smaller crystallites.

**SEM-EDX characterization**

The surface morphology characterization and elemental composition of chitosan and the chitosan–$Al_2O_3$–GO composite (1:3 ratio) were conducted using Scanning Electron Microscopy with Energy Dispersive X-ray Spectroscopy (SEM-EDX). **Figure 3(a)** depicts the surface morphology of unadulterated chitosan. The chitosan surface displays a granular texture, characterized by an irregular particle size distribution, and is predominantly dense and non-porous. This structure is a typical characteristic of chitosan produced via casting or direct drying processes, without the incorporation of pore-forming agents. The minimal porosity of pure chitosan results in a reduced specific surface area, thereby limiting its dye adsorption capacity in the liquid phase [29]. The lack of accessible pores restricts the diffusion of adsorbate molecules to only the external surface of the material.



**(a)** **(b)**

**Figure 3** SEM morphology (a) chitosan and (b) chitosan–$Al_2O_3$–GO with 10,000× magnification.

In contrast, **Figure 3(b)** depicts a significant morphological change resulting from the compositing of chitosan with $Al_2O_3$ and GO. The surface of the chitosan–$Al_2O_3$–GO (1:3) composite exhibits a notably rougher, more heterogeneous structure, characterized by its porosity. Pores ranging from submicron to micrometre size are randomly distributed across the material's surface. This porous network is critical for adsorption performance as it facilitates the diffusion of methylene blue molecules to internal active sites that were previously inaccessible. The morphological changes can be attributed to 2 main mechanisms: (1) the incorporation of $Al_2O_3$ particles, which act as spacers or fillers, creating interfacial cavities within the polymer matrix [30], and (2) the intercalation of GO sheets among the chitosan chains, which disrupts the compact arrangement of the polymer [31]. The synergistic effect of these components results in a more open and accessible surface structure for adsorbate molecules. The wrinkled and crumpled topology introduced by the GO sheets further contributes to increased surface roughness and porosity. The morphological findings are consistent with studies that suggest the incorporation of GO into the polymer matrix can lead to the formation of porous or crumpled structures, which in turn increases the effective surface area.

**Table 2** Composition of elements of chitosan and chitosan–$Al_2O_3$–GO composite.

| Material | Element (%) | | | | | | | |
|---|---|---|---|---|---|---|---|---|
| | C | N | O | Al | S | Na | K | Mn |
| Chitosan | 43.0 | 4.0 | 53.0 | - | - | - | - | - |
| Chitosan–$Al_2O_3$–GO | 60.7 | 3.4 | 27.8 | 0.7 | 0.71 | 1.1 | 1.8 | 3.8 |

EDX analysis was conducted to confirm the elemental composition of the synthesized material. The EDX spectrum of pure chitosan confirms the presence of carbon (C), nitrogen (N), and oxygen (O) as the primary components of the 2-amino-2-deoxy-D-glucose polymer chain. The EDX spectrum of the chitosan-$Al_2O_3$-GO (1:3) composite reveals characteristic peaks for carbon (C), nitrogen (N), and oxygen (O), as well as distinct peaks for aluminium (Al). A summary of the elemental composition is presented in **Table 2**. The presence of the Al peak in the EDX spectrum of the composite clearly indicates the successful integration of $Al_2O_3$ into the composite matrix. Furthermore, a significant increase in the weight or atomic percentage of carbon (C) compared to pure chitosan may suggest the influence of the GO carbon framework. The presence of nitrogen (N) in the composite suggests that the amino functional groups of chitosan are retained, potentially serving as active sites for the binding of cationic dyes through electrostatic interactions or the formation of coordination complexes [32]. These nitrogen-containing groups, together with the hydroxyl groups and the aromatic domains of GO, provide multiple binding mechanisms for methylene blue adsorption. **Table 2** shows that the oxygen value from SEM-EDX is 53%. The high oxygen content in chitosan is due to the use of technical chitosan (impure). The Mn and K contents still detected by SEM-EDX as shown in **Table 2** indicate that the resulting composite still contains impurities originating from the oxidizer remaining from incomplete washing. However, these residual elements are structurally trapped within the composite cross-linked network, minimizing the risk of direct dissolution during the adsorption process. Nevertheless, optimization of the washing protocol remains crucial for future scale-up to ensure absolute environmental safety.

**BET characterization**

The specific surface area and porosity of pure chitosan and the chitosan–$Al_2O_3$–GO (1:3) composite were characterized using the Brunauer-Emmett-Teller (BET) method through nitrogen adsorption-desorption at 77 K. The results of the analysis (**Table 3**) reveal that pure chitosan has a notably low surface area of 7.036 $m^2/g$, a property inherent to this polymer due to its dense chain structure and limited porosity. In contrast, the chitosan–$Al_2O_3$–GO (1:3) composite demonstrated a significant enhancement in surface area, reaching 23.009 $m^2/g$, which is approximately 3.3 times greater. This remarkable increase supports the effectiveness of the modification strategy involving the integration of

$Al_2O_3$ and GO. The synergistic effect of incorporating both $Al_2O_3$ nanoparticles (which act as rigid spacers preventing polymer chain agglomeration) and GO sheets (which provide high surface area carbonaceous platforms) is responsible for this textural improvement. For comparison, Desnelli *et al.* [13] investigation of the binary chitosan–GO (1:1) composite, which lacks $Al_2O_3$, recorded a surface area of 11.60 $m^2/g$. The addition of $Al_2O_3$ as a third component notably improves the surface area, confirming the findings of Kamal *et al.* [33] and Hasan *et al.* [34], which highlighted the positive effects of GO incorporation and inorganic constituents on the surface area of chitosan-based composites.

The analysis of the mean pore size reveals that pure chitosan has a pore diameter of 13.8531 nm, while the composite shows a slightly reduced diameter of 13.1067 nm. The modest reduction in pore size in the composite suggests that the chitosan pores are partially occluded by $Al_2O_3$ particles and GO sheets. Despite this slight decrease, the pore size remains in the mesoporous range which is ideal for liquid-phase adsorption as it provides a balance between surface area and accessibility for dye molecules. The phenomenon a large increase in surface area accompanied by only a slight change in pore diameter suggests that the $Al_2O_3$ particles and GO sheets subdivide large void spaces into a greater number of smaller mesopores, thereby increasing the overall pore population as demonstrated in GO/chitosan-based 3D composites [35]. An increased surface area provides additional active sites for interactions with methylene blue molecules through electrostatic mechanisms, complex formation, or π–π interactions [36]. A well-documented positive correlation exists between surface area and adsorption capacity, suggesting that adsorbents with larger surface areas typically exhibit enhanced adsorption capacities [37]. Collectively, the results confirm that the chitosan–$Al_2O_3$–GO (1:3) composite has improved textural properties compared to pure chitosan and may demonstrate enhanced adsorption efficacy for methylene blue dye.

Although the incorporation of GO increase the specific surface area of the composite from 7.036 to 23.009 $m^2/g$, the obtained value remains considerably lower than the theoretical surface area reported for isolated graphene-based materials. This phenomenon is mainly attributed to the restacking and aggregation of GO sheets during the sol–gel synthesis and drying processes, which reduce the accessibility of internal surfaces to nitrogen molecules during BET measurements. In addition, chitosan chains and $Al_2O_3$ particles may partially occupy interlayer spaces and pore channels of GO, further limiting the accessible surface area. Drying at 80 °C may also induce partial shrinkage of the polymeric network and collapse of some pore structures. Therefore, the measured BET value reflects the accessible surface area of the composite rather than the theoretical surface area of individual GO sheets. Nevertheless, the increase from 7.036 to 23.009 $m^2/g$ confirms that the incorporation of GO and $Al_2O_3$ successfully improved the surface properties of chitosan and contributed to its enhanced adsorption performance [38].

**Table 3** Comparison of the surface area of chitosan and chitosan–$Al_2O_3$–GO composite (1:3).

| Material | Surface Area ($m^2/g$) | Pore size (nm) |
|---|---|---|
| Chitosan | 7.036 | 13.853 |
| Chitosan–$Al_2O_3$–GO (1:3) | 23.009 | 13.106 |

**Study methylene blue adsorption from composite chitosan–$Al_2O_3$–graphene oxide (GO)**

***pH variation on adsorption studies***

Determining the zero-charge point (pHpzc) (**Figure 4(a)**) is essential for comprehending the electrokinetic properties of an adsorbent's surface, as this parameter dictates the surface charge distribution across different pH levels and directly influences the electrostatic interactions between the adsorbent and the adsorbate. The pHpzc value of the chitosan–$Al_2O_3$–GO composite (pH 7.0) is situated between the standard values of pure chitosan (pH ~6.3) and GO (pH ~3.5), indicating that the addition of $Al_2O_3$ and GO has substantially altered the surface properties of chitosan. The shift of pHpzc to a more neutral value compared to pure chitosan reflects the contribution of the acidic

oxygen functional groups from GO and the amphoteric nature of the $Al_2O_3$ surface, which possesses both Lewis acid and base sites. Sheimukhanova *et al.* [39] state that at a pH below the pHpzc, the adsorbent surface exhibits a predominance of positive charges resulting from the protonation of functional groups, while at a pH above the pHpzc the surface acquires a negative charge due to deprotonation.

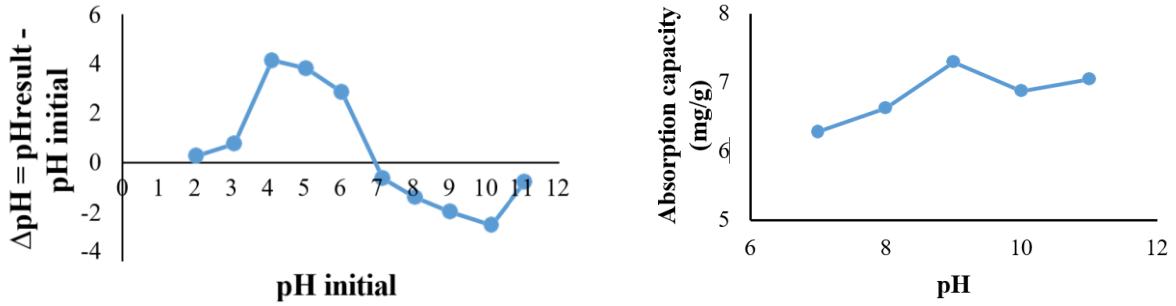



**Figure 4** (a) pHpzc and (b) adsorption capacity from composite on methylene blue.

The investigation into the influence of pH on the adsorption capacity of methylene blue was conducted within a pH range of 7 to 11 (**Figure 4(b)**). The results revealed a significant increase in adsorption capacity from pH 7 to pH 9, followed by a moderate decline at pH 10 and 11. At pH 7, which is close to the pHpzc of the composite, the surface possesses nearly neutral charge characteristics, resulting in relatively weak electrostatic interactions between the adsorbent and methylene blue molecules. Nevertheless, adsorption still occurred due to other possible interactions, including π–π interactions between the aromatic rings of methylene blue and the $sp^2$ carbon domains of graphene oxide, as well as hydrogen bonding involving oxygen-containing functional groups on graphene oxide and hydroxyl or amino groups of chitosan. As the pH increased to 8 and 9, the surface functional groups (−COOH on graphene oxide [GO] and −OH on alumina [$Al_2O_3$] and GO) underwent gradual deprotonation to form $-COO^-$ and $-O^-$ [40]. This condition is thought to increase the electrostatic interaction between the negatively charged adsorbent surface and the cationic methylene blue molecules, resulting in an increased in adsorption capacity that reaches optimum conditions at pH 9. The peak at pH 9 represents an optimal balance: the composite surface is sufficiently negatively charged to maximize electrostatic attraction, while the concentration of hydroxide ions ($OH^-$) is not yet high enough to compete significantly with the anionic binding sites. The decline in adsorption capacity at pH 10 and 11 can be attributed to 2 factors: (1) the increasing concentration of $OH^-$ ions in the solution, which competes with the anionic surface sites for interaction with the cationic methylene blue molecules, and (2) possible partial hydrolysis or structural weakening of the chitosan matrix under strongly alkaline conditions, which may reduce the availability of active sites. These findings are consistent with research by Rahmatpour *et al.* [41] on chitosan/GO hydrogel composites, which reported improved MB adsorption at higher pH levels, and with Luong *et al.* [7], who observed that MB adsorption on GO/chitosan composites also peaked at pH 9.

***Time variation and the kinetic studies adsorption***

The investigation of the contact time effect aimed to determine the optimal duration required for the chitosan–$Al_2O_3$–GO (1:3) composite to reach methylene blue adsorption equilibrium. The experiment was conducted over a period of 10 to 60 min, with 10-minute intervals, under optimal pH conditions of 9 and an initial concentration of 25 mg/L. **Figure 5** shows a gradual increase in adsorption capacity as contact time is extended, reaching a maximum value of 6.708 mg/g at 50 min, with a removal efficiency of 88.39%. The rapid increase in adsorption capacity during the initial phase (10 - 30 min) indicates the presence of numerous active sites on the composite surface and a steep concentration gradient between the solution and the adsorbent surface. This gradient serves as a driving force for the mass transfer of methylene blue molecules to the active sites. This observation is consistent with the fundamental

principle of adsorption, where the initial adsorption rate is primarily influenced by rapid external and internal diffusion, due to the strong affinity of the adsorbate for the adsorbent surface [42]. The increase in adsorption capacity begins to slow down between 40 and 50 min as contact time progresses. This indicates a gradual reduction in the number of available active sites, which are becoming increasingly occupied by methylene blue molecules [43]. The slowing kinetics also suggest a transition from surface-controlled adsorption to intraparticle diffusion, where dye molecules must navigate through the mesoporous network to access binding sites located deeper within the composite matrix.

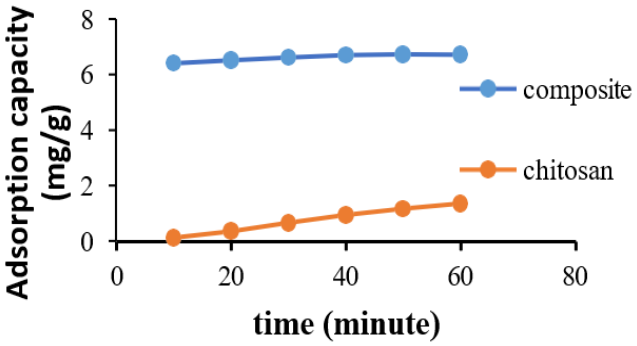



**Figure 5** Effect of contact time variation on methylene blue adsorption by composite.

Adsorption capacity has optimum equilibrium state after 60 min which his reduction is attributed to partial desorption, where some methylene blue molecules that were adsorbed onto the composite surface are reintroduced into the solution. This reintroduction may occur due to shear forces from continuous agitation or the establishment of a dynamic equilibrium between adsorption and desorption processes. Zhang *et al.* [44] noted that the adsorption rate initially increases rapidly before gradually decreasing until equilibrium is reached, as many pores are available for adsorption at first but become less accessible over time. The findings suggest that a contact duration of 50 min is optimal for future adsorption studies. In contrast, pure chitosan demonstrated an adsorption capacity of approximately 1 mg/g under similar conditions, confirming that modification with $Al_2O_3$ and GO significantly enhanced the composite's adsorption effectiveness. This improvement aligns with the increase in specific surface area, which rose from 7.036 $m^2/g$ to 23.009 $m^2/g$, as confirmed by BET analysis.

The mechanism and rate of methylene blue adsorption on the chitosan–$Al_2O_3$–GO composite were investigated by analyzing the experimental kinetic data using 2 predominant kinetic models: The pseudo-first-order (PFO) model by Lagergreen which generally applicable during the initial phase of physical adsorption and the pseudo-second-order (PSO) model by Ho and McKay which applicable during chemical interactions. The kinetic parameters derived from the linear regression analysis of the experimental data are summarized in **Figure 6** and **Table 4**. The findings indicate that the PSO model offers a significantly better fit to the experimental data when compared to the PFO model, with a coefficient of determination ($R^2$) of 0.982 for the PSO model versus 0.966 for the PFO model. Beyond the higher $R^2$ value, 2 additional criteria confirm the superiority of the PSO model: (1) The calculated equilibrium adsorption capacity (Qe(cal)) from the PSO model (6.393 mg/g) shows excellent agreement with the experimental value with a relative error of only 4.7%; (2) the PSO model is mechanistically consistent with the surface chemistry of the composite on chitosan–$Al_2O_3$–GO composite possesses multiple types of functional groups which are capable of forming specific chemical bonds with methylene blue molecules, aligning with the chemisorption assumption inherent in the PSO model. The superior fit of the PSO model provides strong kinetic evidence that chemisorption, rather than mere physisorption, is the rate-limiting step in the adsorption process. This mechanism entails important chemical interactions between the surface functional groups of the adsorbent and the molecules of the adsorbate.

Specifically, it involves electrostatic interactions between the negatively charged surface of the composite (at pH 9) and the cationic methylene blue molecules, the complexation of the amino groups (−$NH_2$) of chitosan with the dye molecules, and π–π interactions between the aromatic rings of methylene blue and the $sp^2$ graphene oxide framework [45,46]. The value of the PSO rate constant ($K_2$ = 0.0039 g/mg.min) is relatively small, which is characteristic of systems where chemical interactions govern the overall rate rather than diffusion processes. This is consistent with the multi-interaction mechanism proposed for this composite, where the formation of electrostatic, π–π, and coordination bonds requires specific molecular orientation and activation energy.

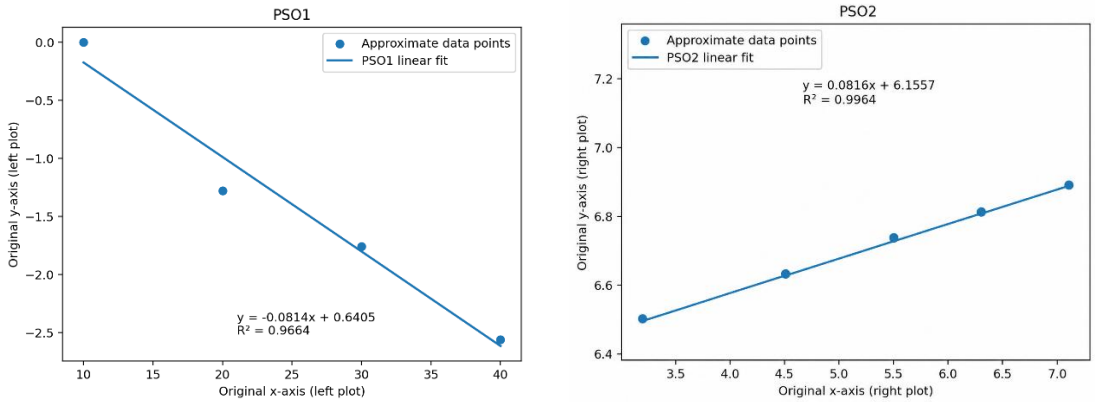



**Figure 6** Pseudo first order and pseudo second order curve for kinetic adsorption.

**Table 4** Study of adsorption kinetic parameters on chitosan–$Al_2O_3$–GO.

| Material | Qe (exp) | Pseudo First Order | | | Pseudo Second Order | | |
|---|---|---|---|---|---|---|---|
| | | Qe(cal) | $K_1$ | $R^2$ | Qe(cal) | $K_2$ | $R^2$ |
| Chitosan–$Al_2O_3$–GO | 6.708 | 1.897 | 0.0814 | 0.966 | 6.393 | 0.0039 | 0.982 |

The close agreement between the experimental Qe (6.708 mg/g) and the calculated Qe from the PSO model (6.393 mg/g) further validates the applicability of this model and supports the conclusion that the adsorption capacity is governed by the availability of chemisorptive binding sites. The prominence of the PSO model in chitosan and graphene oxide (GO)-based composite systems for the adsorption of methylene blue is well-documented in the literature. Luong *et al.* [7] indicated in their study on the adsorption of methylene blue using GO/chitosan composite granules that the adsorption process follows the PSO model, with the intra-particle diffusion mechanism dominating during the first 4 h. Fan *et al.* [47] found that the adsorption kinetics of methylene blue with magnetic chitosan–GO (MCGO) composites closely adhered to the PSO model. The consistency of these findings with existing literature bolsters the validity of the results presented in this study.

**Concentration variation and the adsorption isotherm models**

The influence of initial methylene blue concentration on the adsorption capacity of the chitosan–$Al_2O_3$–GO (1:3) composite was investigated within a concentration range of 20 - 50 mg/L, at an optimal pH of 9 and an ideal contact time of 50 min. The experimental results (**Figure 7**) show a gradual increase in adsorption capacity as the initial adsorbate concentration rises, reaching a maximum value of 10.817 mg/g at a concentration of 45 mg/L, with a removal efficiency of 80.12%. This increase in adsorption capacity can be attributed to the heightened concentration gradient between the solution phase and the adsorbent surface. Higher initial concentrations of methylene blue in the solution significantly increase the frequency of collisions between adsorbate molecules and the active sites on the composite surface, thereby enhancing the adsorption capacity [49]. The concentration gradient acts as the thermodynamic

driving force, overcoming mass transfer resistance and enabling more efficient utilization of the available binding sites. However, at a concentration of 50 mg/L a decrease in adsorption capacity was observed, indicating that the composite had reached saturation levels. All available active sites on the adsorbent surface are occupied by methylene blue molecules, meaning that further increases in adsorbate concentration do not result in significant enhancements in adsorption capacity. In contrast, pure chitosan demonstrates an adsorption capacity of only 1 - 2 mg/g under similar conditions, highlighting that the modification with $Al_2O_3$ and GO has considerably improved the adsorption efficacy of the composite. This notable enhancement can be explained by the synergistic effects of the 3 components: $Al_2O_3$ increases surface area and mechanical stability, GO facilitates π-π interactions and introduces oxygen functional groups, and chitosan provides amino groups as active sites while also serving as a supporting matrix that aids in the separation of the adsorbent after adsorption.

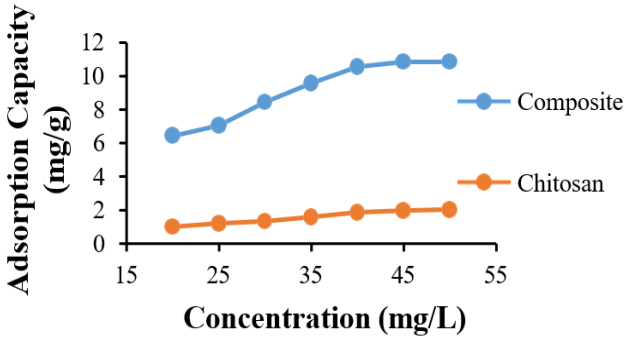



**Figure 7** Effect of initial methylene blue concentration on the equilibrium adsorption capacity of pure chitosan and chitosan–$Al_2O_3$–GO (1:3) composite.

**Table 5** Adsorption isotherm parameter data of chitosan–$Al_2O_3$–GO composite towards Methylene Blue dye.

| Isotherm Models | Parameter Isotherm | Value |
|---|---|---|
| Langmuir | $Q_m$ (mg/g) | 11.60 |
| | $K_L$ (L/mg) | 1.25 |
| | $R^2$ | 0.998 |
| Freundlich | N | 2.91 |
| | 1/n | 4.74 |
| | $K_r$ (mg/g) | 6.75 |
| | $R^2$ | 0.794 |

The adsorption mechanism of methylene blue interacting with the chitosan–$Al_2O_3$–GO composite was elucidated by analyzing the adsorption equilibrium data through the Langmuir and Freundlich isotherm models. The Langmuir model suggests monolayer adsorption on a uniform adsorbent surface, characterized by energetically identical active sites and the absence of intermolecular interactions among the adsorbed species. In contrast, the Freundlich model is an empirical framework that describes multilayer adsorption on a heterogeneous surface with a non-uniform distribution of active site energies. The isotherm parameters obtained from fitting the experimental data are presented in **Table 5**. The analysis shows that the Langmuir model provides a significantly better fit to the experimental data compared to the Freundlich model, with a coefficient of determination ($R^2$) of 0.9978 for Langmuir versus 0.794 for Freundlich. The selection of the Langmuir model as the more appropriate isotherm is justified by 3 independent lines of evidence: (1) the $R^2$ value of 0.998 indicates near-perfect linearity, (2) the Langmuir-derived Qm (11.600 mg/g) is in close agreement with the experimentally observed saturation capacity at 45 mg/L initial concentration confirming the

model's predictive accuracy, (3) the Langmuir assumption of monolayer coverage on a homogeneous surface is physically consistent with the XRD and SEM-EDX characterization. This monolayer behavior suggests that once a methylene blue molecule occupies an active site, that site is effectively blocked, and intermolecular interactions between adsorbed dye molecules are minimal. The uniformity of the surface implied by the Langmuir fit indicates a homogeneous distribution of functional groups across the composite, consistent with the successful dispersion of GO and $Al_2O_3$ within the chitosan matrix as revealed by XRD and SEM. The $R^2$ value approaching 1.0 in the Langmuir model indicates that the adsorption of methylene blue onto the chitosan–$Al_2O_3$–GO composite occurs in a monolayer on a relatively uniform surface. These results confirm that the active sites on the composite surface are evenly distributed and exhibit identical affinity for methylene blue molecules. The maximum adsorption capacity (Qm) derived from the Langmuir model is 11,600 mg/g, accompanied by a Langmuir constant (KL) of 1.25 L/mg. The elevated KL value signifies a strong interaction between the adsorbent and the adsorbate, supporting the presence of various active sites on the composite surface, including carboxyl and hydroxyl groups on GO that are deprotonated at pH 9, amino groups on chitosan, and Lewis acid sites on the $Al_2O_3$ surface. A $K_L$ value greater than 1 indicates a favorable adsorption process with strong binding affinity, consistent with the chemisorptive nature suggested by the PSO kinetic model. The 1/n parameter from the Freundlich model was determined to be 0.2108. A 1/n value between 0.1 and 0.5 generally indicates a favorable adsorption process. However, the low $R^2$ value (0.794) suggests that the Freundlich model poorly represents the adsorption mechanism in this system, making the Langmuir model more appropriate for explaining the adsorption behavior of the chitosan–$Al_2O_3$–GO composite with respect to methylene blue.

The maximum adsorption capacity of the chitosan–$Al_2O_3$–GO composite (11.600 mg/g) is relatively modest compared to certain advanced adsorbents such as CS/$Fe_3O_4$/GO (30.10 mg/g) studied by Taha *et al.* [49] and GO@CS beads (23.26 mg/g) studied by Taha *et al.* [49] and Nayl *et al.* [50], respectively. However, the 5 - 10 fold increase from pure chitosan (1 - 2 mg/g) is a significant achievement. Key advantages of this composite include its straightforward synthesis, the use of cost-effective and eco-friendly raw materials, and the ease of post-adsorption separation facilitated by the chitosan matrix. The chitosan–$Al_2O_3$–GO composite possesses characteristics that make it a promising option for treating textile wastewater, particularly in extracting cationic dyes like methylene blue from solutions with low to moderate concentrations.

Based on the results of visual observations during the adsorption process at various pH, contact time, and initial dye concentration, it was seen that after the adsorption process, the composite showed spontaneous sedimentation ability which was characterized by the formation of solid particle deposits at the bottom of the solution. The composite showed the ability to form sedimentation at the bottom of the system after the adsorption process. The increase in sedimentation ability was caused by the formation of cross-links between chitosan and GO, as well as the presence of $Al_2O_3$ which could reduce the electrostatic repulsion between particles, thus encouraging aggregation and the formation of a composite structure with a larger particle size. The formation of this large aggregate caused the sedimentation process to occur faster [51]. In addition, the sedimentation process occurred spontaneously, namely the solution was left for 60 min to separate completely. In the synthesized GO solution, it showed high dispersion stability and was not easily subjected to spontaneous precipitation and required a longer time to settle. This stability was caused by the presence of oxygen-containing functional groups on the GO surface which were hydrophilic, thus increasing interactions with water molecules and maintaining dispersion through electrostatic repulsion between GO sheets [52]. This causes GO to be difficult to separate from the liquid medium and requires additional processes such as centrifugation to accelerate the separation. In addition, based on previous reports, GO used in the adsorption process was also reported to be difficult to recover after the adsorption process [53]. Modification of GO with chitosan and $Al_2O_3$ can increase the recovery ability of the adsorbent after use in dye adsorption.

A systematic comparison was conducted to contextualize the adsorption performance of the chitosan–$Al_2O_3$–GO composite among recently developed adsorbents. **Table 6** outlines the maximum adsorption capacities (Qm), experimental parameters,

and key practical characteristics of various chitosan- and GO-based adsorbents reported in the literature for the removal of methylene blue. The Qm of the chitosan–$Al_2O_3$–GO composite (11.60 mg/g) is comparable to that of the chitosan-GO hydrogel (12.50 mg/g) reported by Huang *et al.* [40] and significantly exceeds that of pure chitosan (~2.0 mg/g, this study) and γ-$Al_2O_3$ nanoparticles (8.50 mg/g) [9]. While the composite's Qm is lower than that of high-performance magnetic systems like CS/$Fe_3O_4$/GO (30.10 mg/g) [48] and GO@CS beads (23.26 mg/g) [49]. The chitosan–$Al_2O_3$–GO composite offers several notable practical advantages: (i) the synthesis method is straightforward and eliminates the need for expensive magnetic nanoparticles (e.g., $Fe_3O_4$), hazardous crosslinking agents, or energy-intensive hydrothermal processes; (ii) the raw materials by chitosan derived from renewable crustacean waste, readily available alumina, and graphite are cost-effective and environmentally friendly; (iii) the composite can be easily separated from treated water through simple sedimentation or filtration, eliminating the need for external magnetic fields; and (iv) the composite shows a 5 - 10 fold improvement over pure chitosan, demonstrating the effectiveness and synergy of the $Al_2O_3$ and GO modifications. The characteristics of the chitosan–$Al_2O_3$–GO composite position it as a viable and sustainable option for treating low to moderate concentrations of cationic dyes, particularly in situations where operational simplicity, cost-effectiveness, and environmental sustainability are prioritized. Based on that, the chitosan–$Al_2O_3$–GO composite achieves a favorable balance among adsorption efficiency, material cost, and operational feasibility. Its performance surpasses that of the individual adsorbents (chitosan, GO, and $Al_2O_3$), empirically supporting the synergistic effect of the 3 components.

**Table 6** Comparative evaluation of adsorption performance and operational characteristics of chitosan–$Al_2O_3$–GO composite and recently reported adsorbents for methylene blue removal.

| Adsorbent | Qm (mg/g) | Optimal pH | Contact Time (min) | Adsorbent Dose (g/L) | Key Features | Reference |
|---|---|---|---|---|---|---|
| Chitosan–$Al_2O_3$–GO (1:3) | 11.6 | 9 | 50 | 3.33 | Simple synthesis, low-cost, eco-friendly, easy separation | This study |
| Pure chitosan | ~2.0 | 9 | 50 | 3.33 | Biodegradable, low capacity | This study |
| Chitosan–GO hydrogel | 12.5 | 8 | 60 | 2 | High water uptake, good capacity | [40] |
| GO/chitosan composite beads | 23.26 | 9 | 120 | 1 | Granular form, easy separation, higher capacity | [49] |
| CS/$Fe_3O_4$/GO | 30.1 | 9 | 90 | 1.5 | Magnetic separation, high capacity | [48] |
| γ-$Al_2O_3$ nanoparticles | 8.5 | 9 | 60 | 2 | Low cost, moderate capacity | [9] |

## Conclusions

The research findings indicate that the chitosan–$Al_2O_3$–GO composite was successfully synthesized using the sol-gel method. This is supported by XRD analysis, which shows characteristic peaks corresponding to the 3 constituent components, and SEM-EDX analysis, which reveals a porous surface morphology along with the presence of carbon (C), nitrogen (N), oxygen (O), and aluminum (Al) elements in the composite. BET analysis demonstrated a significant increase in specific surface area, rising from 7.036 $m^2/g$ for pure chitosan to 23.009 $m^2/g$ for the chitosan–$Al_2O_3$–GO composite (1:3), with an average pore size of 13.1067 nm, classifying it as mesoporous. The composite also exhibited optimal adsorption performance for methylene blue at a pH of 9 and a contact duration of 50 min, achieving an adsorption capacity of 10.817 mg/g and a removal efficiency of 80.12% at an initial concentration of 45 mg/L. The adsorption equilibrium analysis indicated that the process follows the Langmuir isotherm model ($R^2$ = 0.9978), with a maximum monolayer adsorption capacity of 11.600 mg/g, suggesting a monolayer adsorption mechanism on a homogeneous surface. Furthermore, the adsorption kinetics study revealed that the experimental data fit the pseudo-second-order model

($R^2$ = 0.978) more closely than the pseudo-first-order model ($R^2$ = 0.925) which confirms that the rate-determining steps of adsorption involve chemisorption mechanisms, characterized by electrostatic interactions, complex formation, and π-π interactions between the functional groups of the composite surface and methylene blue molecules. These findings suggest that the chitosan–$Al_2O_3$–GO composite has potential as a low-cost and easily separable adsorbent for textile wastewater treatment. However, regeneration and reusability were not evaluated in this study; therefore, future work should investigate adsorption–desorption cycles and the performance of the composite in real wastewater systems.

**Acknowledgements**

The research/publication of this article, as funded by DIPA of Public Service Agency of Universitas Sriwijaya, Indonesia 2021. Nomor SP DIPA 023.11.2.67751512024, On November 21, 2023. In accordance with the Rector's Decree Number. 00l3/UN9/LP2M.PT/2024, On May 20, 2024.

**Declaration of generative AI in scientific writing**

Generative AI tools were used in this study only to improve the readability and language of the manuscript. All content data interpretation, analysis, and conclusions were produced and verified by the authors. The use of AI-assisted technologies was conducted under full human oversight, and the authors take complete responsibility for the accuracy and integrity of the final text.

**CRediT author statement**

**Desnelli**: Supervision, Writing - original draft, Methodology, Investigation, Formal analysis, Data curation, Conceptualization. **Fadhilah Syafutri**: Methodology, Investigation. **Daniel Alfarado**: Methodology, Investigation, Formal analysis, Writing - original draft. **Eva Musifa**: Project administration, Writing - original draft, Data curation. **Muhammad Said**: Writing - review & editing, Supervision, Resources, Methodology, Funding acquisition, Conceptualization. **Ady Mara**: Writing - review & editing, Visualization. **Suheryanto**: Validation, Methodology, Investigation, Formal analysis. Wiwien Andriyanti: Methodology, Funding acquisition, Conceptualization. **Bayu Mardi Kartika**: Methodology, Investigation, Formal analysis, Data curation, Validation.

**References**

[1] Y Lyu, Y Liu, Y Guo, J Tian and L Chen. Managing water sustainability in textile industry through adaptive multiple stakeholder collaboration. *Water Research* 2021; **205**, 117655.

[2] MM Islam, AR Aidid, JN Mohshin, H Mondal, S Ganguli and AK Chakraborty. A critical review on textile dye-containing wastewater: Ecotoxicity, health risks, and remediation strategies for environmental safety. *Cleaner Chemical Engineering* 2025; **11**, 100165.

[3] ZM Xiong, X Mao, M Trappio, C Arya, JE Kordi and K Cao. Ultraviolet radiation protection potentials of Methylene Blue for human skin and coral reef health. *Scientific Reports* 2021; **11(1)**, 10871.

[4] B Anegbe, IH Ifijen, M Maliki, IE Uwidia and AI Aigbodion. Graphene oxide synthesis and applications in emerging contaminant removal: A comprehensive review. *Environmental Sciences Europe* 2024; **36**, 15.

[5] N Bellier, P Baipaywad, N Ryu, JY Lee and H Park. Recent biomedical advancements in graphene oxide- and reduced graphene oxide-based nanocomposite nanocarriers. *Biomaterials Research* 2022; **26(1)**, 65.

[6] E Adotey, A Kurbanova, A Ospanova, A Ardakkyzy, Z Toktarbay, N Kydyrbay, M Zhazitov, N Nuraje and O Toktarbaiuly. Development of superhydrophobic reduced graphene oxide (rGO) for potential applications in advanced materials. *Nanomaterials* 2025; **15(5)**, 363.

[7] HVT Luong, TP Le, TLT Le, HG Dang and TBQ Tran. A graphene oxide based composite granule for methylene blue separation from aqueous solution: Adsorption, kinetics and thermodynamic studies. *Heliyon* 2024; **10(7)**, e28648.

[8] B Liu, YN Xin, J Zou, FM Khoso, YP Liu, XY Jiang, S Peng and JG Yu. Removal of chromium species by adsorption: Fundamental principles, newly developed adsorbents and future perspectives. *Molecules* 2023; **28(2)**, 639.

[9] A Ali, MI Vohra, A Nadeem, BS Al-Anzi, M Iqbal, AA Memon, AH Jatoi, J Akhtar, J Yang and KH Thebo. Ultrafast graphene oxide-lignin biopolymer nanocomposite membranes for separation of biomolecules, dyes, and salts. *ACS Applied Polymer Materials* 2024; **6(8)**, 4747-4755.

[10] MA Shehab, M Al-lami, MA Taher, HH Mohammed, AA AbdulRazak, KT Rashid, A Mahmood, MF Abd Al-Ogaili and S Alsarayefi. Recent progress in adsorptive removal of different contaminants by chitosan-based aerogel. *RSC Advances* 2025; **15(36)**, 29727-29742.

[11] H Rajabi and SM Jafari. Synthesis and characterization of 3-dimensional graphene oxide-chitosan/glutaraldehyde nanocomposites: Towards adsorption of crocin from saffron. *International Journal of Biological Macromolecules* 2024; **281(4)**, 136672.

[12] TS Vo. Progresses and expansions of chitosan-graphene oxide hybrid networks utilizing as adsorbents and their organic dye removal performances: A short review. *Journal of the Turkish Chemical Society Section A: Chemistry* 2021; **8(4)**, 1121-1136.

[13] D Desnelli, S Safitri, E Musifa, A Hamidah, M Said, S Suheryanto and A Mara. Study of Congo Red adsorption by chitosan-graphene oxide (ChitosanGO) composite synthesize with hydrothermal synthetic method: Optimization and determination condition. *Indonesian Journal of Fundamental and Applied Chemistry* 2025; **10(2)**, 101-111.

[14] MS Akhtar, S Ali and W Zaman. Innovative adsorbents for pollutant removal: Exploring the latest research and applications. *Molecules* 2024; **29(18)**, 4317.

[15] MR Farani, I Zare, M Mirshafiei, A Gholami, M Zhang, E Pishbin, JE Ahn, A Mohammadi, M Imani, M Lak, J Shen, H Kang and YS Huh. Graphene oxide-engineered chitosan nanoparticles: Synthesis, properties, and antibacterial activity for tissue engineering and regenerative medicine. *Chemical Engineering Journal* 2025; **509**, 160852.

[16] D Desnelli, IH Padillah, M Ulfa, E Eliza, A Mara and F Fatma. Synthesis of chitosan-$Al_2O_3$ composite using the sol-gel method and its application in photodegradation of Methylene Blue. *Indonesian Journal of Fundamental and Applied Chemistry* 2023; **8(1)**, 40-47.

[17] N Anuwongsa, T Yawai and W Ananpreechakorn. A simple preparation of graphene oxide with a modified Hummer's method. *Indochina Applied Sciences* 2023; **12(3)**, 251664.

[18] HP Buwono, S Adiwidodo, H Wicaksono and HI Firmansyah. Hydrothermal synthesis and characterization of nano-particles γ-$Al_2O_3$. *IOP Conference Series: Materials Science and Engineering* 2021; **1073**, 012011.

[19] M Sabzevari, DE Cree and LD Wilson. Gas and solution uptake properties of graphene oxide-based composite materials: Organic vs. inorganic cross-linkers. *Journal of Composites Science* 2019; **3(3)**, 80.

[20] D Desnelli, K Ramadhina, D Alfarado, F Fatma, A Mara and M Said. Methylene blue degradation using chitosan-Fe2O3 composite and photo-Fenton. *Revista Colombiana de Química* 2023; **52(2)**, 36-42.

[21] D Desnelli, D Rizkiani, D Alfarado, F Ferlinahayati, H Yohandini, F Fatma, A Mara, S Suheryanto, E Nurnawati, A Hamidah and M Said. Adsorption study on phenol from bentonite doped with zinc oxide: Synthesis, characterization, equilibrium, kinetics, and thermodynamic. *Indonesian Journal of Fundamental and Applied Chemistry* 2024; **9(2)**, 82-95.

[22] AD Meretoudi, I Kalampogias, I Koumentakou, IK Kalavrouziotis, AK Tolkou and GZ Kyzas. Chitosan/montmorillonite/graphene oxide composites for the adsorption of dyes from single-component solutions, binary mixtures, and real textile wastewaters: On understanding the adsorption interactions. *Langmuir* 2025; **41(34)**, 23198-23213.

[23] MA Saraswati, WH Saputera, E Lafina and D Sasongko. Development of $MnO_2$/γ-$Al_2O_3$ catalysts for catalytic ozonation of phenolic wastewater. *South African Journal of Chemical Engineering* 2026; **55**, 417-427.

[24] I Aranaz, AR Alcántara, MC Civera, C Arias, B Elorza, A Heras Caballero and N Acosta.

Chitosan: An overview of its properties and applications. *Polymers* 2021; **13(19)**, 3256.

[25] S Saisa, Z Sartika, Erdiwansyah, Elvitriana and R Mamat. Application of alumina-chitosan modified monolithic activated carbon derived from empty fruit bunches for acid mine drainage treatment. *Kuwait Journal of Science* 2026; **53(2)**, 100559.

[26] AMA Saputra, N Agustina, Amran, Zurnansyah, Samnur and EH Sujiono. Synthesis and characterisation of graphene oxide/chitosan composite membranes from natural waste. *Journal of Physical Science* 2022; **33(3)**, 63-79.

[27] Y Wang, F Yang, T Wu and G Huang. Systematic overview of the preparation, interface characteristics, strengthening mechanisms, and challenges of graphene-reinforced Al matrix composites. *Journal of Materials Research and Technology* 2024; **33**, 7709-7739.

[28] J Chen, AM Chandler, I Külaots, Q Zhang and VL Colvin. Size effects in magnetic separation for rapid and efficient bacteria removal. *Nanoscale* 2026; **18(3)**, 1433-1444.

[29] M Lehocký. Environmental applications of chitosan derivatives and chitosan composites. *Polymers* 2025; **17(19)**, 2583.

[30] I Roato, T Genova, D Duraccio, FA Ruffinatti, DZ Venturini, M Di Maro, A Mosca Balma, R Pedraza, S Petrillo, G Chinigò, L Munaron, G Malucelli, MG Faga and F Mussano. Mechanical and biological characterization of PMMA/$Al_2O_3$ composites for dental implant abutments. *Polymers* 2023; **15(15)**, 3186.

[31] C Santillo, Y Wang, GG Buonocore, G Gentile, L Verdolotti, S Kaciulis, H Xia and M Lavorgna. Hybrid graphene oxide/cellulose nanofillers to enhance mechanical and barrier properties of chitosan-based composites. *Frontiers in Chemistry* 2022; **10**, 926364.

[32] BA Al-Mur and MT Jamal. Eco-friendly dye removal using chitosan: Characterization and kinetic modeling of Methylene Blue and Methyl Orange adsorption. *Polymers* 2026; **18(5)**, 546.

[33] MA Kamal, S Bibi, SW Bokhari, AH Siddique and T Yasin. Synthesis and adsorptive characteristics of novel chitosan/graphene oxide nanocomposite for dye uptake. *Reactive and Functional Polymers* 2017; **110**, 21-29.

[34] MM Hasan, MA Shenashen, MN Hasan, H Znad, MS Salman and MR Awual. Natural biodegradable polymeric bioadsorbents for efficient cationic dye encapsulation from wastewater. *Journal of Molecular Liquids* 2021; **323**, 114587.

[35] MV Reyes-Peces, A Pérez-Moreno, DM de-los-Santos, MdM Mesa-Díaz, G Pinaglia-Tobaruela, JI Vilches-Pérez, R Fernández-Montesinos, M Salido, N de la Rosa-Fox and M Piñero. Chitosan-GPTMS-silica hybrid mesoporous aerogels for bone tissue engineering. *Polymers* 2020; **12(11)**, 2723.

[36] M Ulfa, RF Hanif and NA Sholeha. Surface chemistry and adsorption behavior of Methylene Blue on functionalized carbon materials: A comprehensive study. *Communications in Science and Technology* 2025; **10(2)**, 276-291.

[37] X Yang, H Zhang, S Cheng and B Zhou. Optimization of the adsorption and removal of Sb(III) by MIL-53(Fe)/GO using response surface methodology. *RSC Advances* 2022; **12**, 4101-4112.

[38] CE Flores-Chaparro, CJ Castilho, I Külaots, R Hurt and J Rangel-Méndez. Pillared graphene oxide composite as an adsorbent of soluble hydrocarbons in water: pH and organic matter effects. *Journal of Environmental Management* 2020; **259**, 110044.

[39] L Seimukhanova, U Zhantikeyev, I Sapargali, M Kunarbekova, K Kudaibergenov, E Skwarek and S Azat. Surface and structural characterization of buckwheat husk-derived activated carbons: Correlation of SEM, elemental, FTIR, Raman, and porous properties with electrokinetic behavior. *International Journal of Molecular Sciences* 2026; **27(4)**, 1803.

[40] JQ Huang, K Liu, X Song, G Zheng, Q Chen, J Sun, H Jin, L Jiang, Y Jiang, Y Zhang, P Jiang and W Wu. Incorporation of $Al_2O_3$, GO, and $Al_2O_3$@GO nanoparticles into water-borne epoxy coatings: Abrasion and corrosion resistance. *RSC Advances* 2022; **12(38)**, 24804-24820.

[41] A Rahmatpour, N Alijani and AH Alizadeh. Preparation of chitosan-based ternary nanocomposite hydrogel film by loading graphene oxide nanosheets as adsorbent for enhanced

Methylene Blue dye removal. *International Journal of Biological Macromolecules* 2023; **253(1)**, 126585.

[42] R Maceiras, J Feijoo, L Perez-Rial, MA Alvarez-Feijoo and N Eslami. Influence of activated carbon granulometry on $H_2$ purification in glycerol reforming syngas: Adsorption and kinetic analysis. *Energies* 2024; **17(23)**, 6011.

[43] A Ouzani, Y Zouambia, H Maachou, M Krea, AA Assadi, L Khezami, Y Benguerba, J Zhang, A Amrane, W Elfalleh and H Tahraoui. Sustainable removal of Basic Fuchsine and Methylene Blue dyes using chicken bone biomass: Thermodynamics, kinetics, and insights from experimental studies and decision tree with least squares boosting predictive modeling. *Water* 2025; **17(7)**, 1053.

[44] X Zhang, X Zhang and W Xu. Adsorption performance and mechanism of waste Myriophyllum aquaticum biochar for Malachite Green in wastewater: Batch and column studies. *Sustainability* 2025; 17(7), 2868.

[45] S Ebrahimi, P Zanganeh, S Nouripour-Sisakht, H Javadian, A Babaie, R Khaleghi and A Asfaram. A multifunctional graphene oxide-ZnO nanohybrid for rapid and highly efficient Malachite Green adsorption and strong broad-spectrum antimicrobial activity. *Scientific Reports* 2026; **16(1)**, 7316.

[46] AE Eltaweil, EM Abd El-Monaem, AM Omer, RE Khalifa, MM Abd El-Latif and GM El-Subruiti. Efficient removal of toxic Methylene Blue (MB) dye from aqueous solution using a metal-organic framework (MOF) MIL-101(Fe): Isotherms, kinetics, and thermodynamic studies. *Desalination and Water Treatment* 2020; **189**, 395-407.

[47] L Fan, C Luo, M Sun, X Li, F Lu and H Qiu. Preparation of novel magnetic chitosan/graphene oxide composite as effective adsorbents toward Methylene Blue. *Bioresource Technology* 2012; **114**, 703-706.

[48] J Ren, S Zhang, Y Wang and H Yang. Adsorption properties and mechanisms of Methylene Blue by modified Sphagnum moss bio-based adsorbents. *Materials* 2024; **17(17)**, 4329.

[49] G Taha, RA Baseer and M Sultan. Chitosan nanocomposites for the removal of pollutants from waste water. *Discover Applied Sciences* 2025; **7**, 1306.

[50] AA Nayl, AI Abd-Elhamid, WAA Arafa, IM Ahmed, AA El-Shanshory, MA Abu-Saied, HMA Soliman, MA Abdelgawad, HM Ali and S Bräse. Chitosan-functionalized-graphene oxide (GO@CS) beads as an effective adsorbent to remove cationic dye from wastewater. *Polymers* 2022; **14(19)**, 4236.

[51] F Pinelli, T Nespoli and F Rossi. Graphene oxide-chitosan aerogels: Synthesis, characterization, and use as adsorbent material for water contaminants. *Gels* 2021; **7(4)**, 149.

[52] S Stankovich, RD Piner, X Chen, N Wu, ST Nguyen and RS Ruoff. Stable aqueous dispersions of graphitic nanoplatelets via the reduction of exfoliated graphite oxide in the presence of poly(sodium 4-styrenesulfonate). *Journal of Materials Chemistry* 2006; **16(2)**, 155-158.

[53] M Sabzevari, DE Cree and LD Wilson. Graphene oxide-chitosan composite material for treatment of a model dye effluent. *ACS Omega* 2018; **3(10)**, 13045-13054.